Research Square

Preprints are preliminary reports that have not undergone peer review.
They should not be considered conclusive, used to inform clinical practice,
or referenced by the media as validated information.

Compensating repair-induced core loss in rewound induction motors by constrained winding redesign: a loss-ratio criterion for repair shops

Mert Ekiz

mert.ekiz@std.yildiz.edu.tr

Independent researcher

Research Article

Keywords: induction motor, rewinding, motor repair, core loss, stator winding design, finite-element analysis

Posted Date: November 20th, 2026

DOI: https://doi.org/10.21203/rs.3.rs-11790876/v1

License: This work is licensed under a Creative Commons Attribution 4.0 International License.
Read Full License

Additional Declarations: No competing interests reported.

Compensating repair-induced core loss in rewound induction motors by constrained winding redesign: a loss-ratio criterion for repair shops

Mert Ekiz[1*]

[1*]Independent researcher, Türkiye, ORCID: 0009-0004-8974-4870.

Corresponding author(s). E-mail(s): mert.ekiz@std.yildiz.edu.tr;

Abstract

Burn-off stripping during rewinding can raise the core loss of an induction motor, and repair guidance accepts increases of up to 20 %. This paper asks how much of that loss a redesigned stator winding can recover. A 2D finite-element model of an open-data 3.7 kW four-pole motor is calibrated on no-load and locked-rotor tests and transferred to an equivalent circuit, with which 345 rewinding designs are evaluated under slot-fill, starting-current and torque limits. For this motor, recovering the rated efficiency at a 20 % core-loss increase needs 3.4–4.8 % more copper area, 9–13 % at +50 %, and about 16 % at half load. The need is governed by the core-to-stator-copper loss ratio r. Where the criterion gives $\boldsymbol{a \leq 1.5}$, a first-order loss balance in r reproduces the model within −8 to +3 percentage points (pp) of copper area, and within +0.6 to +2.4 pp for four IE2/IE3 motors of 7.5–110 kW built from published loss data; with second-order flux-feedback terms it overestimated the requirement in every equivalent-circuit case examined. Measured loss segregations of 20 rewound EASA/AEMT motors (one faulty core excluded) show r = 0.37–1.04 and best-practice core-loss changes of −8 to +18 %. For IE2/IE3 motors with $r \approx 0.5$–0.75, a 20 % increase would require 10–17 % more copper, while 5 % copper headroom absorbs only 7–11 % (4–17 % with uncertain inputs). Near the 20 % limit, modern motors therefore depend on keeping core damage small.

Keywords: induction motor, rewinding, motor repair, core loss, stator winding design, finite-element analysis

Nomenclature

Symbol	Meaning
$a = A_{\mathrm{Cu}}/A_{\mathrm{Cu},0}$	copper-area ratio of the new winding to the original
$A_{\max}$	largest copper area the slot admits in a rewind
Δk_{fe}	relative core-loss increase caused by the repair
$r = P_{\mathrm{fe},0}/P_{\mathrm{Cu1},0}$	core-to-stator-copper loss ratio of the motor before repair
$r_2 = P_{\mathrm{Cu2},0}/P_{\mathrm{Cu1},0}$	rotor-to-stator copper loss ratio
$\delta = I_1 R_{\mathrm{s}} \cos\varphi / V$	in-phase stator voltage drop, per unit of phase voltage V
u	relative reduction of stator resistance by the new winding
$\mu = \mathrm{d}\ln I_{\mathrm{m}}/\mathrm{d}\ln E$	slope of the magnetizing characteristic ($\mu = 1$: linear)
$I_{1,0},\ I_{1,\mathrm{d}}$	rated stator current before and after core damage
η_0	rated efficiency before repair
MLT	mean length of turn
$k_N = N/18$	turns per layer relative to the original winding
k_{ins}	insulated lay factor, $\Sigma d_{\mathrm{ins}}^2$ over the net slot area
$L_{\sigma s},\ L'_{\sigma r}$	stator and referred rotor leakage inductance
$L_{3\mathrm{D}}$	3D end-effect inductance (end windings, end rings, skew)
ψ	magnetizing flux linkage per phase (rms)

1 Introduction

When a three-phase squirrel-cage induction motor fails, rewinding the stator is usually cheaper and faster than replacement. In a survey of industrial users, about 40 % of failed motors were rewound each year, and the share grows with motor rating [13]. Earlier studies reported efficiency losses of 1–5 % per rewind [6], but controlled EASA/AEMT studies found that best-practice rewinding keeps efficiency within ±0.2 %, for energy-efficient [6] and for premium-efficiency (IE3) motors [9].

The same studies identify where efficiency is lost or won. Burn-off stripping above about 360 °C for organic, or 400 °C for inorganic, interlaminar insulation can raise core loss, and teeth splayed by forced coil removal can raise stray loss [6]. EASA guidance limits the core-loss increase during repair to 20 % and recommends repairing or replacing the core beyond that [5]. The ANSI/EASA recommended practice asks that the new winding keep the coil extensions no longer and the conductor area the same or larger [10]. A smaller conductor cross-section or a longer mean length of turn (MLT) raises the stator I^2R loss, which was 22–46 % of the total losses of the motors tested in the EASA/AEMT studies [6, 9].

Rewinding is thus also a chance to improve a motor. Aguiar et al. rewound low-power motors with a redesigned winding and measured efficiency gains of 3–4 points with payback below two years [2]. Ferreira proposed a systematic method that redesigns the stator winding of oversized motors for their actual load cycle, adjusting the magnetizing flux and optimizing coil pitch and turns [12]. Closest to the present question, Cao and Bradley tested 23 motors of 5.5–225 kW before and after rewinding. In the 17 motors rewound under controlled instructions, larger conductors and a tighter winding cut stator conductor loss by 5.3 % on average and offset small increases in core and mechanical loss [7]; a 'tight' winding was also noted to compensate in part for higher core and stray-load loss [8]. They asked whether the chance to redesign the machine at rewind is being wasted, but observed that a shop would first need to know how its own stripping process changes the core loss [7].

These works show that compensation is possible, but not how much copper a given core damage requires, which motors can be compensated at all, or how a shop could

decide this from data it has. Aguiar et al. and Ferreira redesign windings to raise the efficiency of motors with intact cores; Cao and Bradley measure the outcome of rewinds but do not relate the copper needed to the core damage. The criterion derived here is, at first order, an elementary balance of stator copper and core loss, which any machine designer could write down. Its value lies elsewhere: in quantifying how far that balance can be exploited under the constraints of a repair shop, in showing which loss ratio decides the answer, and in checking it against a calibrated model and against measured rewinds. This paper answers these questions with a simulation study that uses a fully documented reference machine as a worked example, the 3.7 kW, four-pole CREATOR Case induction motor of TU Graz, whose geometry, winding, materials and test results are openly published [14, 22]. The contributions are:

1. A quantification of the copper area that recovers the original efficiency for a given core-loss increase and end-turn length, under repair-shop constraints: standard wire sizes, an insulated-wire lay factor, unchanged starting and breakdown performance, part load and temperature.
2. A closed-form criterion in the core-to-copper loss ratio, in a first-order form and with second-order flux-feedback terms, checked against the full model on synthetic loss splits, at part load and on four IE2/IE3 motors of 7.5–110 kW built from published loss data [1].
3. The finding, supported by measured before-and-after losses of 20 rewound motors, that core damage near the 20 % limit cannot be offset in IE2/IE3 motors with the copper headroom a rewind typically offers, and a motor-specific efficiency boundary for the core test.

2 Reference machine and data

The CREATOR Case induction motor [14, 22] is a 3.7 kW, 400 V, 50 Hz, four-pole machine with 36 stator slots and 28 rotor bars (Table 1). Its 2D geometry, winding scheme, material data and test results are published under CC BY-NC 4.0, so every input of this study can be traced. The stator carries a double-layer winding with coil pitch 7/9, 18 turns per layer and slot, and two parallel strands of 0.75 mm wire. The machine is a totally enclosed, water-cooled laboratory prototype with 92 embedded temperature sensors, built for benchmarking rather than as a series motor [22]. Its slot fill is low and its modelled efficiency of 78 % is below the IE1 level for its rating. The results of Section 6 are therefore specific to this machine and illustrate the method; Section 7 generalizes them through the loss ratio r to series motors.

The following measurements from [14] are used: no-load tests at 50 Hz (11 voltage levels), locked-rotor tests at 10–50 Hz, the separated core and friction losses, and the stator and rotor resistances at 20 °C identified by the data providers ($R_s = 2.33\ \Omega$ from a dc test, $R'_r = 1.012\ \Omega$ from the locked-rotor test). The dataset contains no rated-load test with sinusoidal supply; Section 4 therefore uses rated speed, not current, as the check of the rated point.

Table 1 Reference machine [14, 22].

Item	Value
Rating	3.7 kW, 400 V (Y), 50 Hz, 4 poles, 1430 rpm, 24.7 Nm, nameplate current 6.9 A
Stator / rotor slots	36 / 28, open rotor slots with round top bar and tapered lower bar
Stator outer diameter / bore / stack length	200 mm / 125.6 mm / 100 mm
Nominal air gap	0.40 mm
Winding	double layer, pitch 7/9, 18 turns per layer, 2 × 0.75 mm, Y, 216 series turns per phase
Coil area per slot (upper + lower layer)	99.7 mm^2, 85.8 mm^2 net of a 0.25 mm liner
Core material / cage	M800-50A / aluminium alloy 6082

3 Finite-element model, calibration and validation

3.1 Geometry, materials and excitation

Because the published DXF drawing contains duplicated entities, the geometry was rebuilt parametrically from one stator and one rotor slot, rotated 36 and 28 times (Fig. 1). The model has about 1.1×10^5 elements. The only simplification is that each rotor bar is extended by 0.05 mm to the rotor surface.

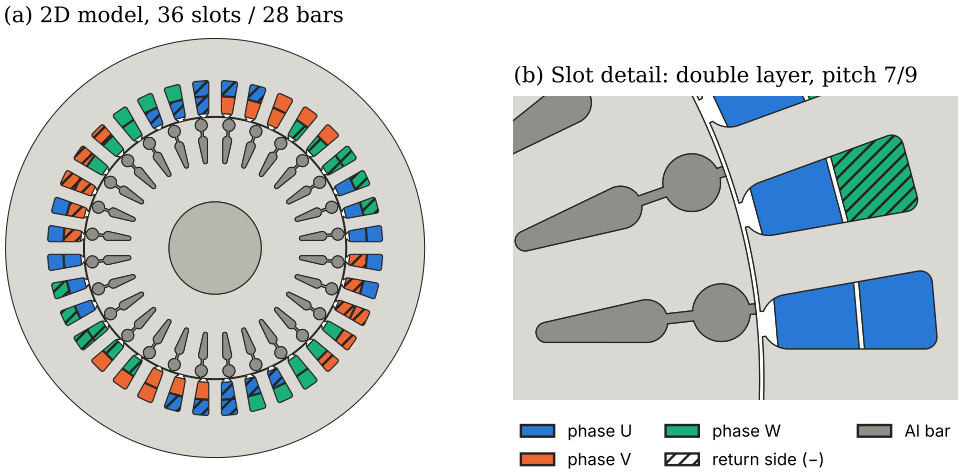


Fig. 1 Rebuilt 2D model of the reference machine with the double-layer 7/9 winding (phase belts coloured) and the 28-bar cage.

The model is solved with FEMM 4.2 [21] driven from Python. The core uses the M800-50A B–H curve of the dataset, extended above 1.7 T with a slope of μ_0. Stator coils are stranded conductors without eddy currents; the stator resistance is taken from measurement. The end-ring resistance is folded into the bar conductivity through

$$K_{\mathrm{ring}} = 1 + \frac{R_{\mathrm{e}}}{2\sin^2(\pi p/N_{\mathrm{b}})\,R_{\mathrm{b}}} = 1.263, \qquad \sigma_{\mathrm{bar}} = \sigma_{\mathrm{Al}}/K_{\mathrm{ring}} \tag{1}$$

where R_b is the resistance of one bar, R_e that of one end-ring segment between two bars, p = 2 and $N_b = 28$; the ring-to-bar current ratio contributes a factor 4, which the two rings halve to 2.

No-load operation is solved magnetostatically at the instant $i_U = \hat{\imath}$, $i_V = i_W = -\hat{\imath}/2$; the phase-U flux linkage gives the synchronous inductance L_s(I). A single rotor position is used; the magnetostatic solution is about ten times faster than a nonlinear time-harmonic one with the same physics at zero slip. Locked-rotor operation is solved time-harmonically at the test frequency; the phase impedance is $\mathrm{Z} = R_s + \mathrm{j}\omega\lambda/\hat{\imath}$ and the cage loss is integrated over the bars.

3.2 Separation of the magnetizing branch from locked-rotor data

At the 2–10 Hz rotor frequencies used to calibrate the cage, the magnetizing reactance is not large against the rotor branch. Following the standard parameter procedures [16, 19], the rotor branch is therefore separated from the locked-rotor impedance before calibration:

$$R_{\mathrm{app}} + jX_{\mathrm{app}} - j\omega L_{\sigma s} = (j\omega L_{\mathrm{m}}) \parallel (R'_{\mathrm{r}} + j\omega L'_{\sigma r}) \tag{2}$$

where $R_{\mathrm{app}} = P/(3I^2) - R_{\mathrm{s}}$ and $X_{\mathrm{app}} = \sqrt{(V/I)^2 - (P/(3I^2))^2}$. L_m is taken from the low-flux no-load data and $L_{\sigma s}$ from equal stator and rotor leakage at 50 Hz, the split also used by the data providers [14]. The same procedure is applied to measured and simulated data; for the measurements it gives $L_{\sigma s} = 9.38$ mH. Omitting the step under-reads R'_r by 7–9 % at 10–50 Hz and about 17 % at 2 Hz; it would give a cage conductivity of 24.5 instead of 29.3 MS/m, a rated slip 22 % too high and an efficiency 0.8 points too low.

3.3 Calibration

Four parameters are calibrated, each on a different test (Table 2). The effective air gap sets the slope of the no-load curve at low flux; the effective lamination fill sets the saturation knee. Scaling the B–H field strength instead was rejected because it degraded the low-flux fit as much as it improved the knee. The cage conductivity is set so that the separated R'_r at 2 Hz, close to the rated slip frequency of 2.3 Hz, equals 1.012 Ω. The 3D end-effect inductance is the difference between the measured and the 2D leakage, split into a stator and a rotor part.

The fill of 0.87 is an effective saturation parameter: it lumps cut-edge damage in the 6.2 mm teeth and deviations of the real laminations from catalogue data, and is not a measured stacking factor.

3.4 Validation

The calibrated model reproduces all 11 no-load points within 2.7 % (Fig. 2); without calibration the error was 7–13 %. After adding the 3D inductance, the total leakage

Table 2 Calibrated parameters.

Parameter	Nominal	Calibrated	Calibrated on
Effective air gap	0.40 mm	0.44 mm	no-load, low flux
Effective lamination fill	0.97	0.87	no-load, saturated region
Cage conductivity	24–32 MS/m	29.3 MS/m	separated R'_r at 2 Hz
3D end-effect inductance	—	2.91 mH (stator), 3.15 mH (rotor)	separated leakage, 10–50 Hz

agrees with the separated measurement within 1.3 % at 10–50 Hz, and the rotor-side 3D term stays between 2.9 and 3.4 mH over that range (Fig. 3). Because the four parameters are calibrated on these tests, the agreement is a calibration fit; the independent checks are the near-constancy of the 3D term with frequency and the rated speed (Section 4).

The model R'_r rises more slowly with frequency than measured (−10 % at 10 Hz, −18 % at 50 Hz). Possible causes are interbar currents, rotor surface losses and skin effect in the end rings, none of which a 2D model captures. This affects starting current and torque, which enter the design study only as constraints relative to the original winding, and not the rated point, where the rotor frequency is 2–3 Hz.

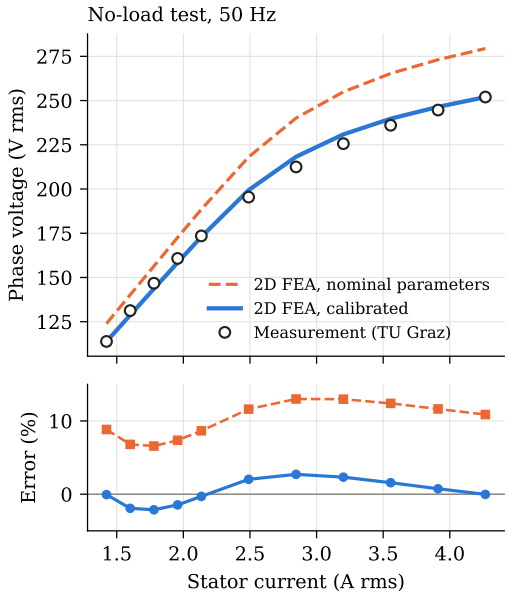


Fig. 2 No-load validation at 50 Hz: measured and calculated phase voltage against current, before and after calibration.

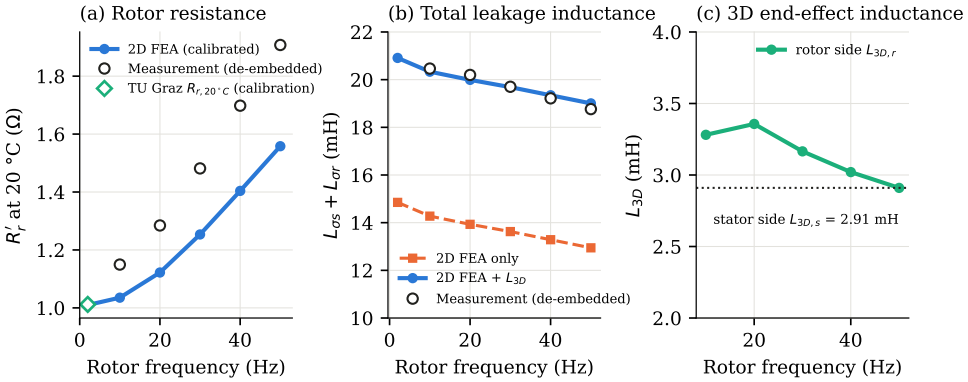


Fig. 3 Locked-rotor validation, 10–50 Hz: (a) rotor resistance at 20 °C after separation of the magnetizing branch ("de-embedded" in the legend), (b) total leakage inductance, (c) rotor-side 3D inductance obtained from the difference.

3.5 Leakage split and saturation at start

Two checks are detailed in Online Resource 1. The FEA puts 33–36 % of the locked-rotor slot energy in the stator; stator shares of 0.30–0.50 change the required copper area by at most 0.006, so the equal split of the standards [16, 19] is kept. At starting currents the 2D leakage reactance saturates to 0.71–0.74 of its low-current value (the 3D term is kept constant); with this saturated leakage the original winding draws 34.4 A instead of 30.9 A, and the 7/9 designs of Table 4 draw 5–7 % more than the original winding.

4 FEA-calibrated equivalent-circuit model

As in earlier work that derives induction-motor equivalent-circuit parameters from 2D field solutions with 3D corrections [11, 20, 24], the calibrated FEA results are transferred to a T-equivalent circuit, which evaluates an operating point in about 5 ms instead of hours of FEA.

- **Magnetizing branch:** the flux linkage $\psi_m(I_m) = (L_s(\mathrm{I}) - L_{\sigma s})\,\mathrm{I}$ from the no-load runs, solved by fixed-point iteration for saturation.
- **Leakage and rotor:** separated $L_{\sigma s}$, $L'_{\sigma r}(f_r)$ and $R'_r(f_r)$ from locked-rotor runs at 2, 10 and 50 Hz, plus the 3D end-effect inductances $L_{3\mathrm{D}}$ of Table 2; one data set for each coil pitch (7/9, 8/9, 9/9).
- **Losses not in the circuit:** core loss from the measured relation $P_{\mathrm{fe}} = 252\ \psi^2 - 6.3$ W at 50 Hz [14] (ψ in Wb, rms), measured between 0.36 and 0.80 Wb (rated point 0.64 Wb; the best designs with 16–17 turns reach 0.68–0.72 Wb, and 14 turns slightly extrapolate to 0.82 Wb) and multiplied by the damage factor $1 + \Delta k_{\mathrm{fe}}$; friction and windage 161 W at 1500 rpm, scaled with speed squared; additional load losses P_{LL} by the assigned value of IEC 60034-2-1:2014 [15], proportional to input

power (kept although the 2024 edition has replaced it, because the efficiency classes of IEC 60034-30-1 [17] refer to it).
- **Temperature:** copper and aluminium at 75 °C in the main study; Section 6.2 adds a thermal feedback.

A rewound stator with N turns per layer is described by $k_N = \mathrm{N}/18$ for the same pitch. Leakage inductances and referred rotor quantities scale with k_N^2, and the magnetizing curve through the MMF, $\psi'(I_m) = k_N\, \psi_m(k_N\, I_m)$. Core loss is evaluated at the physical flux. The stator resistance follows from turns, wire area A_w (n_s parallel strands) and MLT:

$$R_\mathrm{s} = \rho_\mathrm{Cu}(T)\, \frac{N_\mathrm{ph}\, MLT}{n_\mathrm{s}\, A_\mathrm{w}}, \qquad MLT_0 = 0.553 \text{ m} \tag{3}$$

where MLT_0 is calibrated on the measured R_s at 20 °C. A longer coil pitch lengthens the end-turn arc. The increment is not known from the dataset; the main study assumes +5.4 % per slot of pitch (8/9) and +10.7 % for 9/9, and Section 6.4 varies it up to twice that. Starting current and torque are evaluated at standstill, breakdown torque by a slip sweep.

At 3.7 kW the model gives 1436 rpm (rated 1430 rpm) and an efficiency of 78.25 % at 75 °C. The loss split is: stator copper 505 W (49 %), rotor copper 175 W (17 %), friction and windage 148 W (14 %), additional load 104 W (10 %) and core 97 W (9 %), so r = $P_{\mathrm{fe},0}/P_{\mathrm{Cu1},0} = 0.19$. The model current, 7.70 A, is 12 % above the 6.9 A nameplate value; with its reactive part of 3.83 A, anchored by the measured no-load current and leakage, 6.9 A would imply an efficiency of about 93 %, well above what the measured losses allow. The equivalent-circuit parameters published by the data providers [14] give about 7.2 A. Section 6.1 reports how the compensation result changes if the stator copper loss is scaled to 7.2 or 6.9 A.

The gains reported below are larger than a constant-current estimate suggests. For the 2 × 0.85 mm winding, for example, the lower stator drop raises the air-gap EMF: current falls from 7.70 to 7.57 A, slip from 4.25 to 4.05 %, and the stator, rotor and additional load losses fall by 125, 9 and 3 W while core loss rises by 5 W. The net saving is 132 W, or +2.24 points, against 112 W at constant current.

5 Damage scenarios and design space

Damage levels are anchored on repair practice (Table 3). EASA allows at most a 20 % core-loss increase during repair [5, 10]. Lengthening the end turns raises the MLT; with the calibrated MLT_0, the end turns account for about 64 % of a turn (an upper value, since the dc resistance behind MLT_0 includes leads and connections), so a 5 % longer MLT corresponds to about 8 % longer end turns. A 50 % core-loss increase represents a core that exceeds the limit but is rewound anyway. Damage that also lowers permeability is explored as a sensitivity case with FEA at an effective lamination fill of 0.84 and 0.80 (Section 6.5).

The design space covers what a repair shop can wind: 14–20 turns per layer, one to three parallel strands, IEC 60317 nominal diameters from 0.50 to 1.12 mm [18], and coil pitches 7/9, 8/9 and 9/9. Slot filling is judged by the insulated lay factor

Table 3 Damage scenarios.

Scenario	Core-loss factor	MLT factor	Basis
D0 undamaged	1.0	1.00	reference
D1 EASA limit	1.2	1.00	maximum allowed increase [5]
D2 severe	1.5	1.00	core beyond the limit
D3 limit + long end turns	1.2	1.05	about 8 % longer end turns

$$k_{\mathrm{ins}} = \frac{2\,N\,n_{\mathrm{s}}\,d_{\mathrm{ins}}^{2}}{A_{\mathrm{net}}} \tag{4}$$

with n_s parallel strands, d_{ins} the grade-2 maximum overall diameter of the wire [18] and $A_{\mathrm{net}} = 85.8$ mm^2 the coil area per slot net of a 0.25 mm liner. The original winding has $k_{\mathrm{ins}} = 0.57$. Designs are admissible if $k_{\mathrm{ins}} \leq 0.70$ (routine hand insertion) or $\leq$ 0.75 (careful insertion), if the starting current, evaluated with the saturated leakage of Section 3.5, rises by at most 10 %, and if the starting and breakdown torques fall by at most 10 % relative to the original winding. Because these limits are not fixed by a standard, results are also given for $k_{\mathrm{ins}} = 0.65$ and 0.80 (Fig. 6) and for a starting-current limit of 15 %. Grade-2 overall diameters are interpolated linearly between four tabulated sizes, and only windings with $0.40 \leq k_{\mathrm{ins}} \leq 0.80$ are retained. In total 345 windings are evaluated in each of the four scenarios (1,380 operating points).

6 Results

6.1 Compensation map at rated load

Fig. 4 maps the efficiency change against core-loss increase and copper area for the original turn count. The $\Delta\eta = 0$ contour gives the copper area that recovers the undamaged efficiency: 3.4 % more at the EASA limit, 9.1 % at +50 % and 20.8 % at +100 %. A 5 % longer MLT adds 5–6 percentage points of copper area to each value (8.5 %, 14.5 % and 26.8 %), so careless end turns cost more than a core-loss increase at the EASA limit.

These values depend on the motor's stator copper loss, which carries the 12 % current uncertainty of Section 4. Scaling P_{Cu1} to the 7.2 A of the providers' parameters or to the 6.9 A nameplate raises r from 0.19 to 0.23 or 0.26, and the required area at the EASA limit from 1.034 to 1.042 or 1.048 (D2: 1.091 $\rightarrow$ 1.114 or 1.132). The rated-load results are therefore stated as ranges: 3.4–4.8 % at +20 % and 9–13 % at +50 %.

6.2 Part load and temperature

Core loss does not fall with load, so at part load the same damage weighs more against a smaller copper loss. At 75 % load the required area at the EASA limit is 1.071, and at 50 % load 1.156 (D2: 1.204 and 1.517). Fig. 5 shows the consequence for a fixed design: 2 $\times$ 0.85 mm restores the efficiency curve above about 30 % load at +20 % core loss, but at +50 % it stays below the undamaged original below about 65 % load.

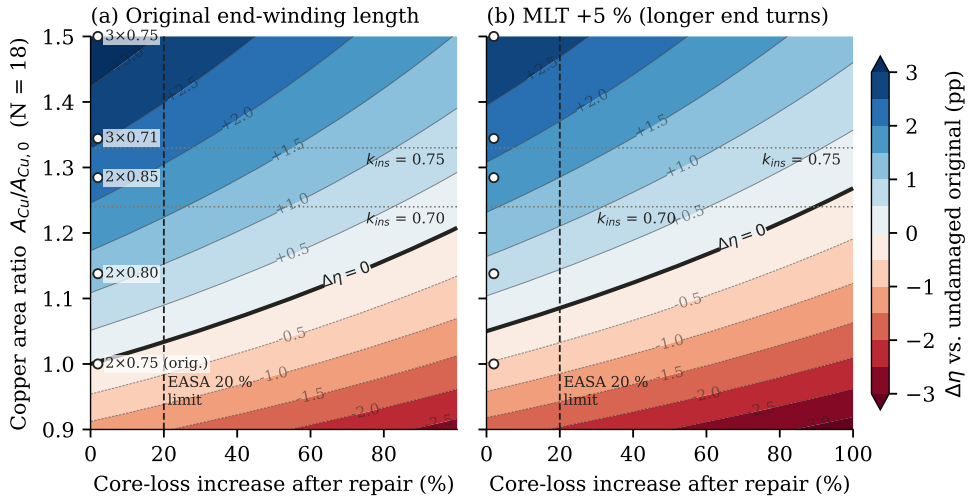


Fig. 4 Efficiency change against core-loss increase and copper-area ratio for 18 turns per layer: (a) original end-winding length, (b) MLT +5 %. The thick line is $\Delta\eta = 0$; circles mark standard wire combinations; dotted lines the copper area reachable at $k_{\mathrm{ins}} = 0.70$ and 0.75 with two strands.

A motor that runs mostly at part load needs more copper than the rated-load map suggests, which supports the recommendation of [7] to consider the operating point at rewind.

A lumped thermal feedback (Online Resource 1) lowers the required area at the EASA limit slightly, to 1.032–1.024 for reference temperatures of 75–115 °C, because a rewind with more copper runs cooler; the fixed-temperature results are therefore conservative.

6.3 Feasible designs

With standard wire sizes, the best admissible 7/9 designs keep 18 turns and add copper through thicker or more strands (Table 4). At $k_{\mathrm{ins}} \leq 0.70$, 3 × 0.67 mm raises efficiency by 1.32 points over the undamaged original at the EASA limit; at $k_{\mathrm{ins}} \leq 0.75$, 2 × 0.85 mm gives 1.88 points. These designs raise the saturated starting current by 5–7 % and the breakdown torque by 8–10 %. Of the 1,380 operating points, 247 are admissible at $k_{\mathrm{ins}} \leq 0.70$ and 271 at $k_{\mathrm{ins}} \leq 0.75$.

Table 4 Efficiency change against the undamaged original (points), coil pitch 7/9, 18 turns, starting-current limit +10 %.

Scenario	Original 2 × 0.75 (k_{ins} 0.57)	3 × 0.67 (k_{ins} 0.69)	2 × 0.85 (k_{ins} 0.73)
D0 undamaged	0.00	+1.67	+2.24
D1 EASA limit	−0.33	+1.32	+1.88
D2 severe	−0.82	+0.79	+1.34
D3 limit + long end turns	−0.84	+0.90	+1.50

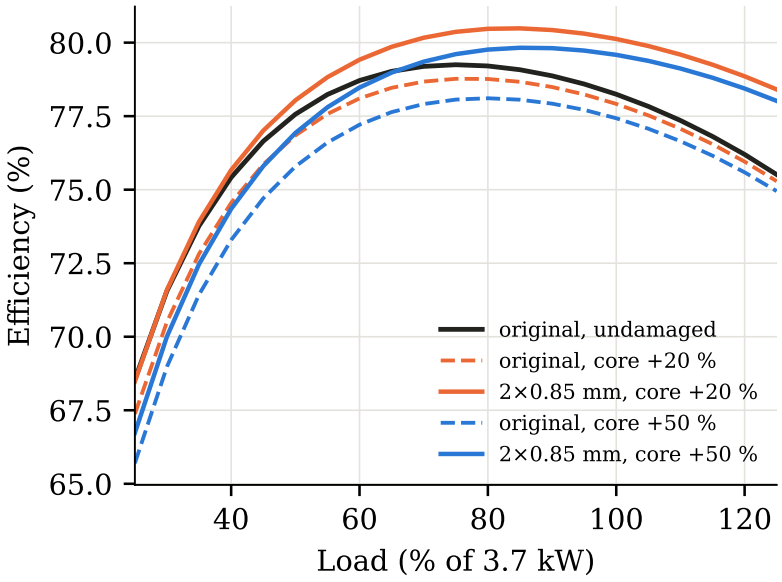


Fig. 5 Efficiency against load for the original winding and the 2 × 0.85 mm rewind at +20 % and +50 % core loss.

The large absolute gains reflect the low original fill of this machine (k_{ins} 0.57, bare-copper fill 37 % of the net area). A factory winding that already fills its slots leaves less headroom; Section 7 treats this case.

6.4 Coil pitch

Fig. 6 shows the best design per pitch against the allowed lay factor at the EASA limit, with saturated starting leakage. Under the 10 % starting-current limit the longer pitches gain nothing: at $k_{\mathrm{ins}} \leq 0.70$ the best 7/9, 8/9 and 9/9 designs give +1.32, +1.35 and +1.32 points, and at $k_{\mathrm{ins}} \leq 0.75$ the original 7/9 pitch is best (+1.88 against +1.45 and +1.69). One turn fewer frees space for copper but raises the starting current. If a 15 % increase is acceptable, 17-turn 8/9 designs drawing 11–12 % more gain 0.4–0.6 points over 7/9 (+1.90 and +2.24), and the 16-turn 9/9 design reaches +2.03 points with 14.7 % more starting current. These margins are of the order of the model's uncertainty in starting current (Section 3.4), so the pitch result is indicative: the pitch is a secondary lever, decided by the starting-current margin of the supply.

Full pitch also loses the short-pitch reduction of the 5th and 7th belt harmonics. Two estimates of their cage loss (FEA and an analytic harmonic circuit [3], Online Resource 1) differ by an order of magnitude but agree that the difference between 7/9 and 8/9 is below 0.08 points; tooth pulsation, rotor-surface losses and interbar currents are not modelled.

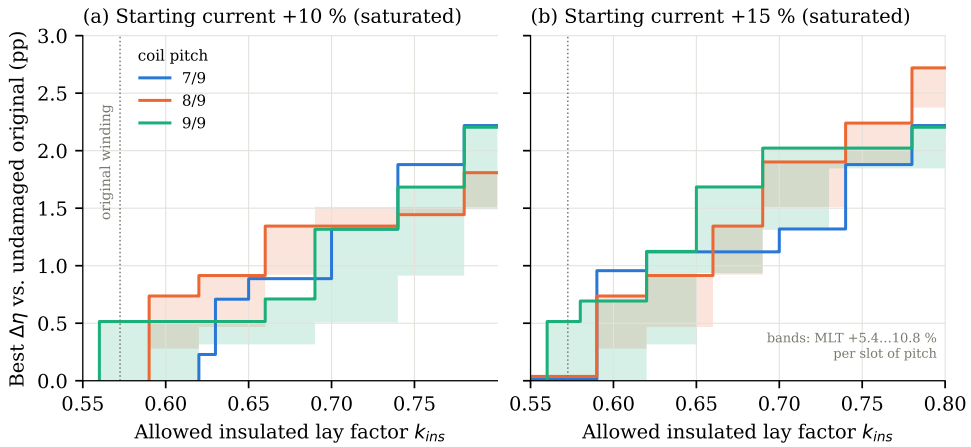


Fig. 6 Best efficiency change per coil pitch against the allowed insulated lay factor, core loss +20 %, starting current evaluated with saturated leakage and limited to (a) +10 % and (b) +15 %. Lines: MLT +5.4 % per slot of pitch; bands: up to +10.8 %.

6.5 Core damage with reduced permeability

Damage that also lowers permeability raises the magnetizing current and adds to the compensation need. The reduced fill is a sensitivity case, not a model of a specific mechanism: burn-off mainly degrades interlaminar insulation, which acts on eddy-current loss. In this case (Online Resource 1), an effective lamination fill of 0.80 instead of 0.87 raises the required area at the EASA limit from 1.034 to 1.067, and the undamaged-core-loss case already needs 2.9 % more copper.

6.6 Uncertainty

A Monte Carlo analysis with 500 samples varied two groups of inputs. Parameter uncertainty: magnetizing curve (±3 %), rotor resistance (σ = 5 %), 2D leakage (±10 %), stator/rotor split of the 3D inductance (30–70 %), core-loss data (σ = 10 %), friction (σ = 15 %) and additional load loss (×0.5–1.5). Model-form uncertainty: stator copper-loss level (scaled to rated currents between 6.9 and 7.7 A) and winding temperature (60–115 °C); the magnetizing curve is re-derived with each leakage sample. The rated efficiency itself is 78.8 % [76.1, 81.1]. The required area at the EASA limit is 1.037 [1.026, 1.053] (median, 95 % interval), at +50 % 1.101 [1.068, 1.147] and with a 5 % longer MLT 1.089 [1.077, 1.105] (Fig. 7a).

The spread is driven by the quantities that set the loss split: stator copper-loss level (Spearman $\rho = -0.60$), core-loss data (0.55) and temperature (−0.47). The FEA calibration parameters, the 3D-inductance split and the leakage inductances all have $|\rho| \leq 0.11$, and the additional load loss $\rho = -0.15$ (Fig. 7b). A repair shop measures the core-loss increase with a loop test at a set yoke flux density, which is not the same as the motor's whole core loss at rated flux. Adding a factor of 0.7–1.3 between the two widens the interval to [1.023, 1.061] and makes it the dominant input ($\rho = 0.73$).

The compensation need is thus a property of the motor's loss split and of how well the core damage is measured, which motivates the criterion of Section 7.

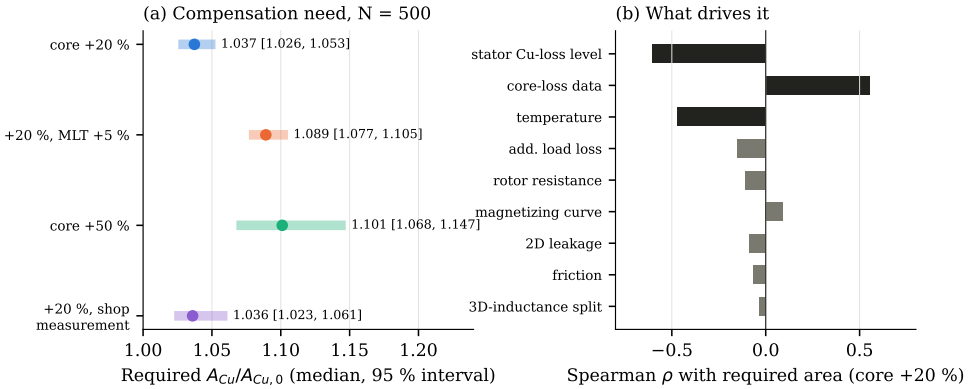


Fig. 7 Monte Carlo analysis, N = 500: (a) required copper-area ratio (median, 95 % interval), including a case with the loop-test-to-motor mapping uncertainty; (b) Spearman rank correlation of the inputs with the required area at the EASA limit.

7 A loss-ratio criterion for repair shops

7.1 Derivation

At constant output, the original efficiency returns when the repair adds no net loss. To first order, the stator copper loss scales with the MLT ratio, with the square of the current ratio and inversely with the copper-area ratio a; with all other losses unchanged, balancing $P_{\mathrm{Cu1}} + P_{\mathrm{fe}}$ before and after repair gives

$$a \approx \frac{MLT}{MLT_0} \left(\frac{I_{1,\mathrm{d}}}{I_{1,0}} \right)^2 \frac{1}{1 - \Delta k_{\mathrm{fe}}\, r} \tag{5}$$

where $I_{1,d}/I_{1,0}$ is the rise of rated current caused by reduced permeability (1 if the core loses no permeability). This first-order form is the shop rule. A lower stator resistance also reduces the stator voltage drop and raises the air-gap EMF by about δu, where u is the relative reduction of stator resistance and $\delta = \mathrm{I}_1 R_s \cos\varphi/\mathrm{V}$ the in-phase drop. Three second-order effects follow. Core loss rises with EMF squared, by $2\delta\mathrm{u}(1 + \Delta k_{\mathrm{fe}})P_{\mathrm{fe},0}$. At constant torque the slip and rotor copper loss fall by 2δu $P_{\mathrm{Cu2},0}$. At break-even the input power, and hence the active current, is unchanged, but the magnetizing current rises by $\mu\delta$u, with $\mu = \mathrm{d}\ \ln I_m/\mathrm{d}\ \ln \mathrm{E}$ (1 for a linear magnetizing branch, 1.6 for the reference motor at rated load); this raises the stator copper loss by $2\mu \sin^2\varphi\ \delta\mathrm{u}\ P_{\mathrm{Cu1},0}$. Including all three gives

$$a \approx \frac{MLT}{MLT_0}\left(\frac{I_{1,\mathrm{d}}}{I_{1,0}}\right)^2 \frac{1}{1-u}, \qquad u = \frac{\Delta k_{\mathrm{fe}}\, r}{1 - 2\delta\left[(1+\Delta k_{\mathrm{fe}})\, r - r_2 + \mu \sin^2\varphi\right]} \tag{6}$$

For modern motors δ is about 0.009–0.03, and the bracket term changes a by less than 0.01 at +20 % and by up to 0.02 at +50 % (Table 5); it matters most for small, low-efficiency motors and at part load. Eq. (6) assumes that the reactive stator current is magnetizing current, $I_1 \sin\varphi \approx I_m$, and its second-order term is derived for $I_{1,\mathrm{d}} = I_{1,0}$; the current-ratio factor is carried over from Eq. (5) as a first-order extension. Both forms require $\Delta k_{\mathrm{fe}}\, r < 1$, and Eq. (6) also $u < 1$: beyond that, the added core loss exceeds the entire original stator copper loss and no copper area restores the efficiency. Inverting the first-order form with $a = A_{\max}/A_{\mathrm{Cu},0}$ gives the largest core-loss increase a rewind can absorb for a given copper headroom:

$$\Delta k_{\mathrm{fe,max}} \approx \frac{1}{r}\left(1 - \frac{MLT}{MLT_0}\,\frac{A_{\mathrm{Cu},0}}{A_{\max}}\right) \tag{7}$$

All inputs are available to a shop: r and r_2 from the measured hot stator resistance with nameplate current, nameplate slip and typical loss shares for the motor's class and rating [1]; δ from nameplate current and power factor; Δk_{fe} from the before-and-after core test.

7.2 Accuracy

The criterion was checked against the full model in three ways (Fig. 8a). First, the hybrid model was re-run with 12 loss splits, r = 0.09–1.24, obtained by scaling either the core loss (by 0.5–6.5) or the stator resistance (by 0.25–1.6), each at $\Delta k_{\mathrm{fe}} = 0.2$, 0.5 and 1.0 and MLT factors 1.00 and 1.05 (72 cases). Second, the reference motor was evaluated at 50 % and 75 % load, with the load-specific ratio. Third, four motors were built from published data: IE2 and IE3 motors of 7.5 kW and IE3 motors of 37 and 110 kW, with efficiencies at the IEC 60034-30-1 minimum [17] and loss shares from the fits of Aarniovuori et al. for four-pole cast-iron motors [1] (Table 5). Their equivalent circuits reproduce these loss shares at an assumed power factor of 0.83 (7.5 kW), 0.86 (37 kW) and 0.87 (110 kW) and a stator and rotor leakage of 0.07 per unit each. The magnetizing branch is linear in the main case. With a saturating branch, $I_m \propto E^{\mu}$ with $\mu = 1.6$ (the reference motor at rated load) or 2.5, the required copper area changes by at most 0.008 and the absorbable core-loss increase at 5 % more copper by at most 0.3 points; both forms of the criterion stay conservative for these motors at rated load.

A shop needs the additional copper, $a - 1$, so the errors are given as the difference between criterion and full model in percentage points (pp) of copper area. For the synthetic splits where Eq. (6) predicts $a \le 1.5$ (n = 44), Eq. (5) errs by −8.0 to +3.2 pp (mean absolute error 1.4 pp) and Eq. (6) by +0.4 to +8.7 pp (mean 2.9 pp). For the reference motor at 50–100 % load the errors are −6.5 to +1.6 pp and +0.8 to +4.8 pp. For the four IE2/IE3 motors the forms nearly coincide, +0.6 to +2.4 pp and +0.7 to +4.0 pp, overstating the increment by 3–8 % and 4–11 % of its value. Eq. (7)

underestimates the absorbable core-loss increase by 0.2–0.8 pp for these motors at 5 % headroom (up to 1.4 pp at 10 %) and by 4 pp for the reference motor.

Eq. (5) is thus the better estimate for modern motors, and Eq. (6) an upper estimate: it overstated the requirement in every case with a finite model solution. Beyond $a \approx 1.5$, however, Eq. (5) underestimates increasingly (1.99 against 2.20 for $r = 0.50$, $\Delta k_{\mathrm{fe}} = 1.0$), and in eight cases it returns a finite, often very large area where the model finds no compensating design: six in the synthetic family that inflates the core loss of the reference motor to efficiencies of 70–74 %, and two copper-scaled cases at $\Delta k_{\mathrm{fe}}\, r = 0.97$, where Eq. (5) gives $a \approx 40$. None resembles a modern motor, but Eq. (5) should be used only for moderate damage. All these checks use equivalent-circuit models that share the criterion's premises (fixed additional load loss and temperature, core loss proportional to ψ^2); they show that second-order circuit effects are small, not that the premises hold. Section 7.4 compares the premises with measurements.

Table 5 Reference motor and four motors built from published loss data [1, 17] and the copper-area ratio a needed to recover their rated efficiency, full model and criterion Eqs. (5) and (6), with the largest core-loss increase absorbable with 5 and 10 % more copper (full model).

Motor	η_0 %	r	r_2	δ	a, +20 % core loss model	(5)	(6)	a, +50 % core loss model	(5)	(6)	$\Delta k_{\mathrm{fe,max}}$ (%) at Cu +5 %	+10 %
Reference 3.7 kW	78.3	0.19	0.35	0.082	1.034	1.040	1.042	1.091	1.106	1.113	29.1	54.6
IE2 7.5 kW	88.7	0.49	0.62	0.026	1.100	1.108	1.110	1.298	1.322	1.331	10.6	20.1
IE3 7.5 kW	90.4	0.60	0.55	0.021	1.128	1.135	1.138	1.402	1.424	1.441	8.5	16.1
IE3 37 kW	93.9	0.63	0.56	0.013	1.139	1.145	1.147	1.445	1.463	1.475	7.8	14.9
IE3 110 kW	95.4	0.73	0.59	0.009	1.166	1.172	1.174	1.561	1.580	1.592	6.7	12.8

7.3 Consequences for repair practice

The reference motor, with r = 0.19 and a low original fill, can absorb large damage: 5 % more copper offsets a 29 % core-loss increase. Motors of 7.5–110 kW cannot (Fig. 8b, Table 5). Their core loss is 16–19 % and their stator copper loss 25–32 % of total losses [1], so r ≈ 0.5–0.75, within the measured 0.37–1.04 of Section 7.4. At the EASA limit they need 10–17 % more copper; with 5 % headroom they absorb only 7–11 %. At part load r rises to 0.77–1.20 (75 % load) and 1.23–2.10 (50 % load), and a 20 % core-loss increase needs 18–31 % and 34–74 % more copper; Eq. (5) stays within +0.4 and −1.6 pp of the model there. A shop should therefore evaluate r at the load where the motor actually runs.

The inputs are uncertain in practice. With ±15 % scatter in the loss shares and a factor of 0.7–1.3 between the loop-test reading and the motor's core loss, the absorbable increase with 5 % more copper is 8.0 % by Eq. (7) (8.5 % with the full model) and 4.8–14.0 % as a 95 % interval for the IE3 7.5 kW motor, 6.5 % (6.7 %), 3.9–11.4 % for the IE3 110 kW motor, and 9.8 % (10.6 %), 5.8–17.2 % for the IE2 7.5 kW motor. The factor 0.7–1.3 is an assumption: loop tests and core testers give comparable readings only when the same procedure is used before and after stripping [4, 23], and the reading does not show whether the damage lies in the yoke or the

teeth. A shop should compare readings of the same tester at the same flux, and add damage concentrated in the teeth, which also raises stray-load loss [8], to $\Delta k_{\mathrm{fe}}\, r$ as an equivalent loss per unit of the original stator copper loss.

Whether 5 % headroom is available depends on the factory winding; the reference motor's lay factor of 0.57 is atypically low. In the measured rewinds of Section 7.4 the corrected winding resistance changed by −10.4 to +9.1 % (median +0.5 %), rose in 11 of 20 motors and fell by 3.7 % or more in only 6. Cao and Bradley's 5.3 % lower stator conductor loss [7] corresponds, by our estimate, to at most about 5.6 % more area, since shorter end turns and lower temperature contribute. A 5 % headroom is therefore an optimistic but achievable case; with less, the conclusion for modern motors becomes stronger. Fig. 8b gives the absorbable damage for any headroom; at $r = 0.6$, each 1 % of extra copper area offsets about 1.6 % of core-loss increase.

These results describe an efficiency boundary, not a replacement for the EASA limit, which also guards against hot spots and insulation stress and reflects the repeatability of core tests [9]. The criterion adds a motor-specific reading of the same test: for r ≈ 0.6 and 5 % headroom, a measured increase above about 8 % (5 % at the lower end of the 95 % interval) cannot be recovered by the winding. Since the core testers in [9] scattered considerably, a reliable before-and-after core test is the limiting input, more than the accuracy of the criterion.

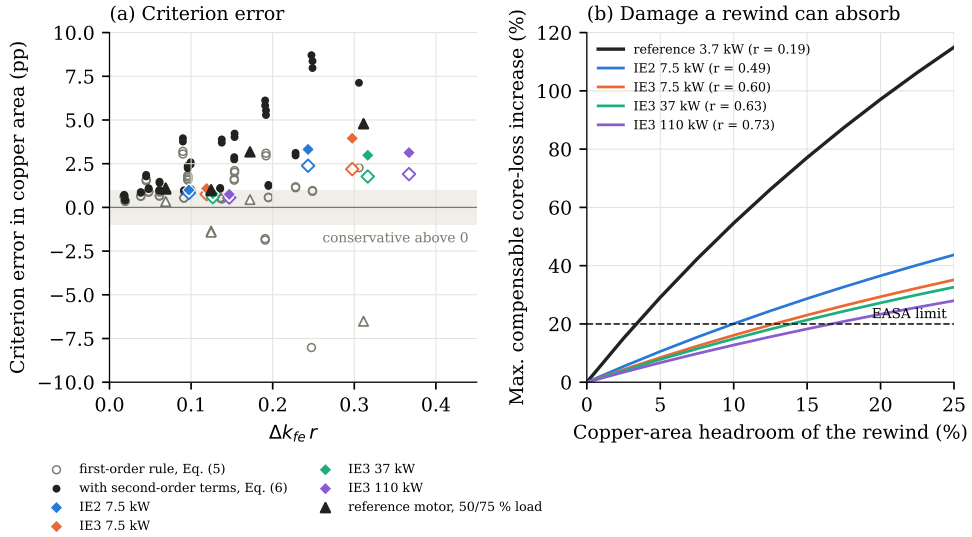


Fig. 8 (a) Error of Eq. (5) (open) and Eq. (6) (filled) against the full model, in percentage points of copper area (positive = overstated; band ±1 pp; synthetic splits where Eq. (6) gives $a \leq 1.5$). (b) Largest core-loss increase offset by a given copper-area headroom, full model.

7.4 Comparison with measured rewinds

The EASA/AEMT studies report IEEE 112B loss segregations before and after rewinding for 10 IE3 motors of 30–75 kW (2019) and 11 motors of 45–150 kW (2003) [6, 9]; the 2019 tests were reported in 2021. These data test the premises of the criterion independently of any model (Fig. 9).

First, the measured loss ratio of these motors is r = 0.37–1.04, median 0.62 (one motor with a faulty core excluded), which confirms the range used in Section 7.3. The seven two-pole motors have a somewhat higher ratio (median 0.76) than the thirteen four-pole motors (median 0.60), so the four-pole IE motors of Table 5 are, if anything, favourable cases. Second, under best-practice repair the core-loss change was −8 to +18 %, median +1 %; only the motor with a core fault from new exceeded 20 % (+48 %). The 2019 losses are reported to about 10 W, so changes of a few percent in core loss are at the resolution of the IEEE 112B segregation, and the median mainly shows that best practice causes no systematic damage. Applying Eq. (5) to the measured r and core-loss increase of each motor, 17 of the 20 would have needed at most 5 % more copper to offset the core damage; the other three (2019 motors G and D, 2003 motor 24E) would have needed 5.6, 7.4 and 12.6 %. Third, the stator I^2R loss rose after rewinding in 9 of the 20 motors even under best practice, so copper headroom is not automatic. In the six motors whose corrected winding resistance fell by 3.7–10.4 % (2003 motors 16H, 18G, 19H, 20H and 21J, and 2019 motor H; smaller reductions are within the test resolution), the stator I^2R loss fell on average 1.1 times as much, which is consistent with the lower current and temperature predicted by the model (about 1.1), although with a scatter of 0.5–1.7 times the data cannot distinguish it from simple proportionality. Finally, the changes of stator I^2R and core loss explain only part of the measured efficiency change: rotor, friction and stray losses together varied about as much as stator I^2R and core loss combined (standard deviations 0.19 and 0.18 % of input). The criterion thus covers the core damage a winding can offset; it does not replace good practice for bearings, fans and stray loss.

8 Discussion and limitations

The study is simulation-based; experimental verification is future work. Its conclusions rest on relative changes, which are far less uncertain than the absolute efficiency (Section 6.6), and on a criterion checked beyond the reference motor.

- **No rated-load measurement.** The 12 % current uncertainty is carried as a range in all rated-load results and as a model-form input in the Monte Carlo analysis.
- **Independence of the criterion check.** The synthetic splits and the IE2/IE3 motors are equivalent-circuit models. Section 7.4 checks the premises against measured loss segregations, but a controlled experiment with deliberate core damage and a redesigned winding remains open.
- **Additional load loss.** The IEC assigned value cannot follow winding changes, and repair can change stray loss in either direction [8]; tooth damage can be included in $\Delta k_{\mathrm{fe}}\, r$ as an equivalent loss.

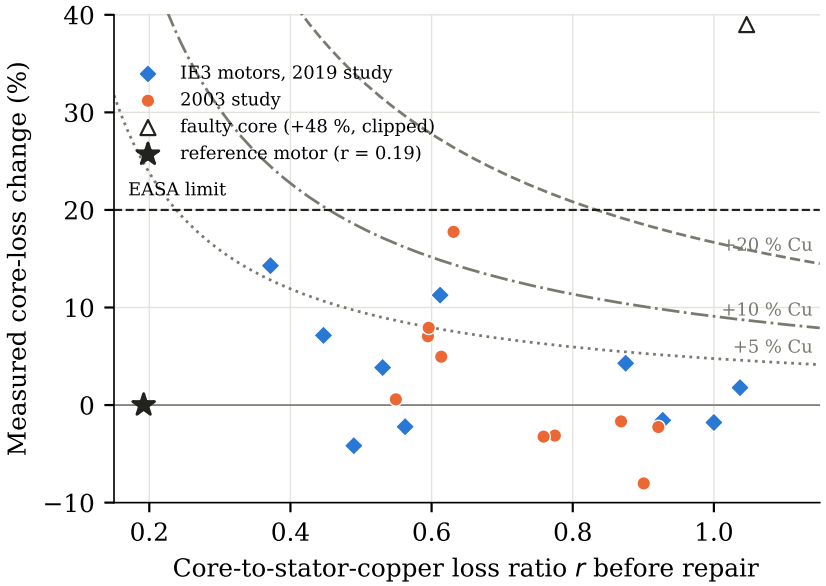


Fig. 9 Measured loss ratio and core-loss change of rewound motors from the EASA/AEMT studies of 2003 [6] and 2019 [9] (six of the 2003 motors and 2019 motor D are two-pole), with the core-loss increase that 5, 10 and 20 % more copper can offset (Eq. (5), MLT unchanged). The star marks the model value of the reference motor, not a measurement.

- **Model simplifications.** The lay-factor limits are engineering judgements (results for 0.65–0.80 in Fig. 6); skew and end-winding leakage are not separable from the data but scale with k_N^2; R'_r is calibrated at 2 Hz and 10–18 % low at 10–50 Hz, so starting current and torque are used only as relative constraints; winding temperature is lumped.
- **Local core damage.** The criterion treats core damage as a global loss increase. Shorted laminations cause hot spots that shorten insulation life, which a loss balance cannot detect; hot-spot inspection and the core-test tolerance [9, 10] remain necessary.

9 Conclusions

A redesigned stator winding can offset repair-induced core loss, but how much depends on the motor's loss split. A calibrated 2D FEA model of the open-data 3.7 kW reference motor, combined with an equivalent circuit and checked against IE2/IE3 motors and measured rewinds, shows that:

1. For the reference motor, 3.4–4.8 % more copper area recovers the rated efficiency at the EASA 20 % core-loss limit and 9–13 % at +50 %; a 5 % longer mean turn adds 5–6 percentage points of copper area, and at half load the need rises to 16 %.
2. The need is governed by the core-to-copper loss ratio r. Where the criterion gives $a \leq 1.5$, a first-order loss balance reproduces the full model within −8 to +3

percentage points (+0.6 to +2.4 for four IE2/IE3 motors of 7.5–110 kW) and underestimates beyond; with second-order flux-feedback terms it overstated the requirement in every equivalent-circuit case examined.

3. For IE2/IE3 motors ($r \approx 0.5$–0.75), a 20 % core-loss increase needs 10–17 % more copper at rated load and more at part load, where r is higher. A rewind with 5 % copper headroom absorbs only 7–11 % (4–17 % as a 95 % interval), and even that headroom is optimistic: the winding resistance fell by 3.7 % or more in only 6 of 20 measured best-practice rewinds. The inverted criterion gives a motor-specific efficiency boundary for the core test that complements the thermal and hot-spot purpose of the 20 % limit.
4. With saturated starting parameters and a 10 % starting-current limit, the original 7/9 pitch remains the best or equal choice; 8/9 with one turn less gains 0.4–0.6 points only if about 12 % more starting current is acceptable.

Acknowledgements. The author thanks the CREATOR team at TU Graz for the open machine data.

Declarations

- **Funding** The author received no funding for this work.
- **Competing interests** The author declares no competing interests.
- **Ethics approval and consent to participate** Not applicable.
- **Consent for publication** Not applicable.
- **Data and code availability** All FEA scripts, results and analysis code are available at https://github.com/ekiztech/rewinding-im-study and archived on Zenodo, doi:10.5281/zenodo.24354574. The machine data are from [14] (CC BY-NC 4.0).
- **Supplementary information** Online Resource 1 gives details of Sections 3.5, 6.2, 6.4 and 6.5.
- **Author contribution** M.E. is the sole author and carried out all of the work: conceptualization, methodology, software, finite-element simulations, formal analysis, investigation, data curation, visualization, and writing (original draft, review and editing).
- **Use of AI tools** The research question, the choice of reference machine and the direction of the study are the author's. The author built and ran all finite-element simulations in FEMM, chose the damage scenarios, design constraints and validation data, and directed each revision. A large language model (Claude, Anthropic) was used as an assistant for code development, analysis scripting, drafting and language editing of the manuscript. The author checked all code, derivations and results against the simulation data, revised the text, and takes full responsibility for the content.

References

[1] Aarniovuori L, Niemelä M, Pyrhönen J, et al (2018) Loss components and performance of modern induction motors. In: International Conference on Electrical

Machines (ICEM), pp 1253–1259, https://doi.org/10.1109/ICELMACH.2018.8507189

[2] Aguiar VPB, Pontes RST, Ferreira FJTE (2018) Technical and economic evaluation of efficiency improvement after rewinding in low-power induction motors: a Brazilian case. Energies 11(7):1701. https://doi.org/10.3390/en11071701

[3] Alger PL (1970) Induction Machines: Their Behavior and Uses, 2nd edn. Gordon and Breach, New York

[4] Bishop T (2003) Proper use of the core tester. EASA Resource Library, Electrical Apparatus Service Association, St. Louis, MO

[5] Bishop T (n.d.) Applying the best of repair best practices: rewind study continues to pay off with important tips. EASA Resource Library, Electrical Apparatus Service Association, St. Louis, MO. https://easa.com/resources/resource-library/applying-the-best-of-repair-best-practices-rewind-study-continues-to-pay-off-with-important-tips, accessed 18 Nov 2026

[6] Bishop TH (2003) EASA/AEMT study of motor repair impact on efficiency. In: ACEEE Summer Study on Energy Efficiency in Industry

[7] Cao W, Bradley KJ (2006) Assessing the impacts of rewind and repeated rewinds on induction motors: is an opportunity for re-designing the machine being wasted? IEEE Transactions on Industry Applications 42(4):958–964. https://doi.org/10.1109/TIA.2006.876069

[8] Cao W, Bradley KJ, Allen J (2006) Evaluation of additional loss in induction motors consequent on repair and rewinding. IEE Proceedings – Electric Power Applications 153(1):1–6. https://doi.org/10.1049/ip-epa:20050144

[9] EASA, AEMT (2021) The effect of repair/rewinding on premium efficiency/IE3 motors. Tech. rep., Electrical Apparatus Service Association, St. Louis, MO

[10] EASA AR100 (2020) ANSI/EASA AR100-2020, Recommended Practice for the Repair of Rotating Electrical Apparatus. EASA

[11] Faiz J, Sharifian MBB, Feyzi MR, et al (2002) A complete lumped equivalent circuit of three-phase squirrel-cage induction motors using two-dimensional finite-elements technique. IEEE Transactions on Energy Conversion 17(3):363–367. https://doi.org/10.1109/TEC.2002.801729

[12] Ferreira FJTE (2023) Optimized rewinding of oversized induction motors. In: IEEE International Electric Machines and Drives Conference (IEMDC), https://doi.org/10.1109/IEMDC55163.2023.10238885

[13] Hasanuzzaman M, Rahim NA, Saidur R, et al (2011) Energy savings and emissions reductions for rewinding and replacement of industrial motor. Energy 36(1):233–240. https://doi.org/10.1016/j.energy.2010.10.046

[14] Heidarikani K, Dhakal PK, Mütze A, et al (2024) CREATOR case: Induction motor data. TU Graz Repository, CC BY-NC 4.0, https://doi.org/10.3217/kh3v7-dhn98

[15] IEC 60034-2-1 (2014) IEC 60034-2-1:2014, Rotating electrical machines – Part 2-1: Standard methods for determining losses and efficiency from tests. IEC, replaced by IEC 60034-2-1:2024

[16] IEC 60034-28 (2012) IEC 60034-28:2012, Rotating electrical machines – Part 28: Test methods for determining quantities of equivalent circuit diagrams for three-phase low-voltage cage induction motors. IEC

[17] IEC 60034-30-1 (2014) IEC 60034-30-1:2014, Rotating electrical machines – Part 30-1: Efficiency classes of line operated AC motors (IE code). IEC

[18] IEC 60317-0-1 (2013) IEC 60317-0-1:2013, Specifications for particular types of winding wires – Part 0-1: General requirements – Enamelled round copper wire. IEC

[19] IEEE 112 (2017) IEEE Std 112-2017, IEEE Standard Test Procedure for Polyphase Induction Motors and Generators. IEEE

[20] Ling Z, Zhou L, Guo S, et al (2014) Equivalent circuit parameters calculation of induction motor by finite element analysis. IEEE Transactions on Magnetics 50(2):833–836. https://doi.org/10.1109/TMAG.2013.2282185

[21] Meeker D (2015) Finite Element Method Magnetics, Version 4.2. https://www.femm.info

[22] Mütze A, Heidarikani K, Dhakal PK, et al (2025) CREATOR case: PMSM and IM electric machine data for validation and benchmarking of simulation and modeling approaches. arXiv:2501.15921, https://doi.org/10.48550/arXiv.2501.15921

[23] Yung C (2009) Core testing: a good procedure gone astray? In: EASA Convention

[24] Zhou P, Gilmore J, Badics Z, et al (1998) Finite element analysis of induction motors based on computing detailed equivalent circuit parameters. IEEE Transactions on Magnetics 34(5):3499–3502

Supplementary Files

This is a list of supplementary files associated with this preprint. Click to download.

- OnlineResource1.pdf